

Isotopic effects in structural properties of graphene

Carlos P. Herrero and Rafael Ramírez

Instituto de Ciencia de Materiales de Madrid, Consejo Superior de Investigaciones Científicas (CSIC), Campus de Cantoblanco, 28049 Madrid, Spain

(Dated: September 4, 2020)

Isotopic effects are relevant to understand several properties of solids, and have been thoroughly analyzed along the years. These effects may depend on the dimensionality of the considered solid. Here we assess their magnitude for structural properties of graphene, a paradigmatic two-dimensional material. We use path-integral molecular dynamics simulations, a well-suited technique to quantify the influence of nuclear quantum effects on equilibrium variables, especially in cases where anharmonic effects are important. Emphasis is put on interatomic distances and mean-square displacements, as well as on the in-plane area of the graphene layer. At low temperature, the relative difference in C–C distance for ^{13}C and ^{14}C , with respect to ^{12}C , is found to be -2.5 and -4.6×10^{-4} , respectively, larger than in three-dimensional carbon-based materials such as diamond. For the in-plane area, the relative changes amount to -3.9 and -6.9×10^{-4} . The magnitude of anharmonicity in the lattice vibrations is estimated by comparing the internal energy and atomic vibrational amplitudes with those derived from a harmonic approximation.

I. INTRODUCTION

In the last years there has been a surge of interest in carbon-based materials, especially in those composed of C atoms with sp^2 hybridization, such as fullerenes, carbon nanotubes, and graphene, a two-dimensional (2D) crystal with extraordinary electronic [1, 2], elastic [3], and thermal properties [4–6]. The structural pattern for pure defect-free graphene corresponds to a honeycomb lattice, but deviations from this flat structure can appreciably affect its atomic-scale and macroscopic properties [7]. In fact, thermal fluctuations at finite temperatures give rise to out-of-plane vibrations of the C atoms, and for $T \rightarrow 0$ the graphene sheet cannot be strictly planar due to zero-point motion.

Anharmonic effects in condensed matter have been studied since many years, because they are responsible for important effects such as thermal expansion, pressure dependence of the compressibility, and phonon couplings, along with the isotope dependence of structural properties and melting temperature [8–10]. In this line, the effect of isotopic composition on the electronic properties, structural parameters, and lattice dynamics of three-dimensional (3D) materials, as well as low-dimensional compounds has been studied with great detail [11–14]. More recently, several isotopic effects have been evaluated in graphene by using various techniques, e.g., vibrational spectroscopy [15, 16] and in particular Raman scattering [17–19]. Moreover, detailed studies about the effect of the atomic mass on the thermal conductivity of graphene have been reported by several research groups [20–23],

Different types of isotopic effects have been analyzed in materials, mainly those caused by the change of phonon frequencies with the atomic mass [12]. This mass dependence of the frequencies gives rise to variations in the vibrational amplitudes. Although at high temperatures the amplitudes are almost independent of the atomic mass, at low temperatures they increase as the mass is lowered,

due to quantum zero-point motion. A larger amplitude *notices* more effectively the anharmonicity of the interatomic potential, thereby yielding a mass-dependence for several structural and thermodynamic properties.

Atomistic simulations (molecular dynamics and Monte Carlo) have been used to study structural and thermodynamic properties of graphene. These simulations were performed using several types of *ab-initio* [24, 25], tight-binding [26–28], and empirical interatomic potentials [29–33]. In most cases, C atoms were treated as classical particles, which is reliable at high temperatures, in the order or larger than the Debye temperature of the material. For graphene, this temperature is rather high: $\Theta_D^{\text{out}} \gtrsim 1000$ K for out-of-plane vibrational modes [34, 35] and $\Theta_D^{\text{in}} \gtrsim 2000$ K for in-plane modes [34, 36].

As isotopic effects on structural variables of crystalline materials are caused by the quantum character of the atomic nuclei and the anharmonicity of the interatomic potentials, a suitable theoretical method to treat this problem is the Feynman path-integral method, a powerful approach to the statistical mechanics of many-body quantum systems at finite temperatures. In particular, the path-integral molecular dynamics (PIMD) technique is well established as a procedure to study many-body problems where anharmonic effects are nonnegligible. Path-integral simulations have been used earlier to study isotopic effects in condensed matter, and were especially applied to analyze the dependence of lattice parameters and thermodynamic properties of solids upon the mass of their constituent atoms [37–40]

In this paper, we study graphene by PIMD simulations between 50 and 1500 K, using an effective interatomic potential, the so-called LCBOP-II, which has been found to reliably describe several structural and thermodynamic properties of this 2D material [30, 41, 42]. This allows us to analyze in a quantitative fashion the influence of isotopic mass on structural properties such as interatomic distances and area of the graphene layer. We consider the most abundant ^{12}C isotope, as well as ^{13}C and ^{14}C .

The anharmonicity of the vibrational modes is assessed by comparing the atomic mean-square displacements derived from PIMD simulations with those obtained from a harmonic approximation.

The paper is organized as follows. In Sec. II, we present the general background to study isotopic effects in structural properties of condensed matter. In Sec. III we describe the computational method used in our calculations. In Sec. IV we present our results for the internal energy, and in Sec. V we discuss the atomic mean-square displacements of the C atoms. Isotopic effects in the interatomic distances and in the in-plane area of the graphene sheet are displayed in Secs. VI and VII, respectively. The paper closed with a summary in Sec. VIII.

II. GENERAL BACKGROUND

For a one-dimensional harmonic oscillator of frequency ω and mass M , the classical mean-square displacement (MSD) at temperature T is given by $(\Delta x)^2 = k_B T / M \omega^2$. Since the vibrational frequency scales with the mass as $M^{-1/2}$, then $(\Delta x)^2$ is independent of M . In a quantum formulation, $(\Delta x)^2$ depends on M , and in the ground state one has $(\Delta x)^2 = \hbar / 2M\omega$, so $(\Delta x)^2 \propto M^{-1/2}$, and the MSD grows for decreasing mass. In both harmonic cases (classical and quantum), the mean position $\langle x \rangle$ does not change with temperature [43]. The same happens for a harmonic description of phonons in solids, so it cannot predict any thermal expansion or isotopic effects in equilibrium structural properties [8, 9].

Here we are interested in the dependence of structural properties of graphene on isotopic mass. Such a dependence does not appear in classical calculations, even in the presence of anharmonicity. This is known for 3D solids, and can be straightforwardly seen from arguments of statistical mechanics. The canonical partition function (NVT) for N particles of mass M arranged in a crystalline 3D solid with volume V at temperature T is given by [44, 45]:

$$Z_{NVT} = \frac{1}{h^{3N}} \int_{V^N} d\mathbf{r}^N \int_{R^{3N}} d\mathbf{p}^N \exp[-\beta H(\mathbf{r}^N, \mathbf{p}^N)], \quad (1)$$

where $\beta = 1/k_B T$, $\mathbf{r}^N = (\mathbf{r}_1, \dots, \mathbf{r}_N)$ and $\mathbf{p}^N = (\mathbf{p}_1, \dots, \mathbf{p}_N)$ are the coordinates and momenta of the particles, and R is the real axis. The Hamiltonian is

$$H(\mathbf{r}^N, \mathbf{p}^N) = \sum_{i=1}^N \frac{\mathbf{p}_i^2}{2M} + U(\mathbf{r}^N), \quad (2)$$

where the first and second term on the r.h.s. are the kinetic and potential energy. In a classical model, the kinetic energy can be integrated out to yield:

$$Z_{NVT}^{\text{cl}} = \frac{1}{h^{3N}} \left(\frac{2\pi M}{\beta} \right)^{3N/2} \int_{V^N} d\mathbf{r}^N \exp[-\beta U(\mathbf{r}^N)]. \quad (3)$$

This means that equilibrium properties that depend only on the coordinates \mathbf{r}^N are independent of the mass M , as this variable appears only in the prefactor of the integral and disappears when taking average values of functions of the coordinates. Thus, for example, the mean-square displacement of particle i is given by $(\Delta r_i)^2 = \langle \mathbf{r}_i^2 \rangle - \langle \mathbf{r}_i \rangle^2$, and does not change with the mass M .

In quantum statistical physics, however, positions and momenta do not commute, so the kinetic energy part in the Hamiltonian cannot be integrated out and the mass M affects the average values of position-dependent variables, as for example $(\Delta r_i)^2$. The same arguments are valid for 2D materials such as graphene. Note that in this case the integration for the space coordinates \mathbf{r}^N is restricted to a limited area in the graphene plane, and is unrestricted in the out-of-plane direction (see below), but this fact does not alter our conclusion.

In summary, isotopic effects in equilibrium structural properties of 2D and 3D materials are pure quantum effects, as they do not appear in classical-like calculations. Moreover, they are typical anharmonic effects, like thermal expansion, and do not show up in the absence of anharmonicity in the interatomic potentials.

As mentioned in the Introduction, several studies based on classical atomistic simulations have been devoted to study structural, dynamic, and elastic properties of graphene in equilibrium conditions at finite temperatures [29, 33]. These methods are, however, useless to study isotopic effects as they are insensitive to the atomic mass. Then, a procedure such as those based on quantum path integrals is necessary for this purpose. Apart from quantum atomistic simulations, another method used earlier to study isotopic effects in solids is the quasi-harmonic approximation (QHA) [46–48]. This procedure has been found to yield reliable results in several studies of solids, and will be employed here to interpret some trends of the results of our simulations. However, a detailed calculation of isotopic effects using the QHA is out of the scope of this paper.

III. COMPUTATIONAL METHOD

A. Path-integral molecular dynamics

In this paper we use the PIMD method to obtain equilibrium properties of graphene at several temperatures for different isotopic masses. This procedure relies on the path-integral formulation of statistical mechanics, a nonperturbative method to study many-body quantum systems at finite temperatures [49]. It profits from the fact that the partition function of a quantum system may be expressed in a form equivalent to that of a classical one, resulting from replacing each quantum particle by a ring polymer made of N_{Tr} (Trotter number) classical particles (*beads*), joined by harmonic springs with constant $k_{\text{har}} = MN_{\text{Tr}}/\beta^2 \hbar^2$ [50, 51]. Details on this simulation technique are given elsewhere [50–52].

We employ the molecular dynamics method to sample the configuration space of the classical isomorph of our quantum system (N carbon atoms). The dynamics in this computational procedure is artificial, as it does not coincide with the quantum dynamics of the actual particles under consideration. This procedure is, however, well suited for adequately sampling the many-body configuration space, yielding accurate results for time-independent equilibrium properties of the quantum system.

The Born-Oppenheimer surface for the nuclear dynamics is obtained from a long-range carbon bond-order potential, LCBOP-II [53–55], which has been used earlier to perform classical simulations of diamond [54], graphite [54], liquid carbon [56], and more recently graphene [29, 33, 57, 58]. For graphene, in particular, this effective potential has been found to give a good description of elastic properties such as Young’s modulus [57, 59]. Also, at 300 K it predicts a bending modulus $\kappa = 1.6$ eV [30], close to the best fit to experimental and theoretical results obtained by Lambin [60].

The calculations presented here were performed in the isothermal-isobaric ensemble, where one fixes the number of carbon atoms (N), the applied in-plane stress (here $P = 0$), and the temperature (T). We used effective algorithms for carrying out PIMD simulations in this statistical ensemble, as those described in the literature [61–63]. We employed staging variables to define the bead coordinates, and the constant-temperature ensemble was generated by coupling chains of four Nosé-Hoover thermostats to each staging variable. An additional chain of four barostats was coupled to the area of the simulation box to yield the required zero pressure [52, 62].

The equations of motion have been integrated by using the reversible reference system propagator algorithm (RESPA), which permits to define different time steps for the integration of fast and slow degrees of freedom [64]. For the time step associated to the interatomic forces we took $\Delta t = 1$ fs, which gave an adequate convergence for the studied variables. For the evolution of the fast dynamical variables (thermostats and harmonic bead interactions), we used $\delta t = \Delta t/4$, as in previous PIMD simulations [14, 65]. The kinetic energy E_{kin} has been calculated by using the so-called virial estimator [62, 66].

The configuration space was sampled at temperatures between 50 K and 1500 K for the carbon isotopes ^{12}C , ^{13}C , and ^{14}C . In each case, we have considered isotopically pure graphene. We have checked that isotopic effects corresponding to mixtures of carbon isotopes coincide within error bars with the values obtained from linear interpolation of the results for isotopically pure samples. To analyze the dependence of several variables on the isotopic mass M , we carried out additional PIMD simulations for several values of M which do not correspond to actual carbon isotopes. Moreover, for comparison with the results of our quantum simulations, some classical molecular dynamics (MD) simulations were also carried out (this corresponds in our context to setting $N_{\text{Tr}} = 1$). We note that the classical limit for equilib-

rium properties can be also reached in the high-mass limit ($M \rightarrow \infty$), as the force constant k_{har} between beads diverges and all the beads corresponding to a particle (here atomic nucleus) collapse into a point, therefore the spatial quantum delocalization vanishes. In our PIMD simulations the Trotter number was taken proportional to the inverse temperature, so that $N_{\text{Tr}} T = 6000$ K, which roughly keeps a constant precision for the PIMD results at different temperatures [14, 65, 67].

We have considered rectangular simulation cells with $N = 960$ and similar side length in the x and y directions of the (x, y) reference plane, and periodic boundary conditions were assumed. For a given temperature, a simulation run consisted of 2×10^5 PIMD steps for system equilibration, followed by 4×10^6 steps for the calculation of ensemble average properties. Some simulations were carried out for $N = 240$ and 448, and the results for the isotopic effects agreed within error bars with those found for $N = 960$.

B. Mean-square displacements

PIMD simulations may be used to analyze the atomic spatial delocalization at finite temperatures. This includes thermal (classical) motion, and a delocalization due to the quantum nature of the atomic nuclei, which can be measured by the spreading of the quantum paths. For a given path, one can define the center-of-gravity (centroid) as

$$\bar{\mathbf{r}}_i = \frac{1}{N_{\text{Tr}}} \sum_{j=1}^{N_{\text{Tr}}} \mathbf{r}_{ij}, \quad (4)$$

where $\mathbf{r}_{ij} \equiv (x_{ij}, y_{ij}, z_{ij})$ is the 3D position of bead j in the ring polymer associated to nucleus i . Hence, the mean-square displacement $(\Delta r_i)^2$ in a PIMD run is given by

$$(\Delta r_i)^2 = \frac{1}{N_{\text{Tr}}} \left\langle \sum_{j=1}^{N_{\text{Tr}}} (\mathbf{r}_{ij} - \langle \bar{\mathbf{r}}_i \rangle)^2 \right\rangle, \quad (5)$$

where $\langle \dots \rangle$ means an ensemble average.

The quantum delocalization of a particle is related in our context to the spread of the paths associated to it, which can be measured by the mean-square *radius-of-gyration* Q_i^2 of the ring polymers:

$$Q_i^2 = \frac{1}{N_{\text{Tr}}} \left\langle \sum_{j=1}^{N_{\text{Tr}}} (\mathbf{r}_{ij} - \bar{\mathbf{r}}_i)^2 \right\rangle. \quad (6)$$

The total MSD of nucleus i at temperature $T > 0$ includes, apart from Q_i^2 , another term corresponding to motion of the centroid $\bar{\mathbf{r}}_i$, i.e.

$$(\Delta r_i)^2 = Q_i^2 + C_i^2, \quad (7)$$

with $C_i^2 = \langle \bar{\mathbf{r}}_i^2 \rangle - \langle \bar{\mathbf{r}}_i \rangle^2$. This term C_i^2 is a semiclassical thermal contribution to $(\Delta r_i)^2$, as it converges at high temperature to the MSD given by a classical model ($Q_i^2 \rightarrow 0$).

For graphene, we call (x, y) the coordinates on the plane defined by the simulation cell, and z the out-of-plane direction. Then, we have expressions like those given above for each direction x , y , and z . For example, $Q_i^2 = Q_{i,x}^2 + Q_{i,y}^2 + Q_{i,z}^2$. In the results presented below, we will show data for the in-plane MSD, defined as an average for the N atoms in the simulation cell:

$$(\Delta r)_p^2 = \frac{1}{N} \sum_{i=1}^N [(\Delta x_i)^2 + (\Delta y_i)^2]. \quad (8)$$

Similarly, one can define an average MSD $(\Delta z)^2$ in the out-of-plane direction [42].

IV. INTERNAL ENERGY

Here we present and discuss the internal energy for graphene made up of different carbon isotopes, as derived from our isothermal-isobaric ensemble for external stress $P = 0$ and several temperatures. In a classical calculation, one finds for the zero-temperature limit a planar graphene surface with an interatomic distance of 1.4199 Å. This corresponds to the minimum-energy configuration with the atomic nuclei fixed on their equilibrium sites without spatial delocalization, and defines the energy E_0 , which is taken as a reference for our calculations at finite temperatures. In a quantum formulation, zero-point motion induces out-of-plane atomic fluctuations in the low-temperature limit, and the graphene layer is not strictly planar. Moreover, anharmonicity of in-plane vibrations gives rise to a zero-point bond dilation, causing an expansion of the graphene lattice, which will be discussed below.

In Fig. 1 we show the internal energy, E_{int} , of graphene as a function of temperature for the different carbon isotopes: ^{12}C (circles), ^{13}C (squares), and ^{14}C (diamonds), where symbols represent results of PIMD simulations. These simulations give separately the potential (E_{pot}) and kinetic (E_{kin}) inputs to the internal energy [52, 62, 66], so for $P = 0$ we have $E_{\text{int}} = E - E_0 = E_{\text{kin}} + E_{\text{pot}}$. Note that most of the internal energy corresponds to the vibrational energy associated to in-plane and out-of-plane modes of graphene. A small part of the potential energy corresponds to the *elastic* energy, which appears for changes in the in-plane area of graphene, mainly at high temperatures (an anharmonic effect) [42].

The internal energy for ^{12}C is found to converge at low T to 171 meV/atom, which gives the zero-point energy of the system. For heavier isotopes we find at low temperature an energy shift of -7 and -13 meV/atom for ^{13}C and ^{14}C , respectively. For comparison, we also show in Fig. 1 results of the internal energy found in classical MD simulations (dashed line). These data are very close

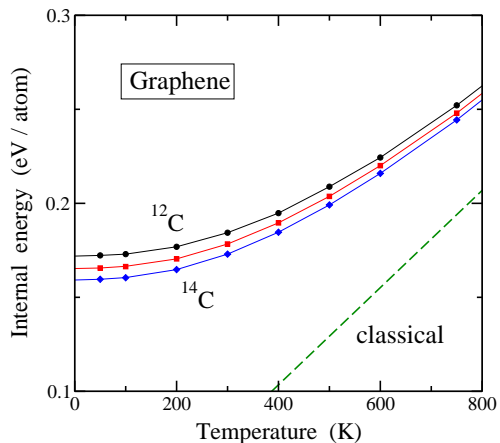


FIG. 1: Temperature dependence of the internal energy of graphene in the region up to 800 K. Symbols represent simulation results obtained for ^{12}C (circles), ^{13}C (squares), and ^{14}C (diamonds). Error bars are smaller than the symbol size. Solid lines are guides to the eye. The dashed line displays the classical vibrational energy per atom: $E_{\text{vib}} = 3k_B T$.

to the classical harmonic expectancy, i.e., $E_{\text{int}}^{\text{cl}} = 3k_B T$ per atom. At high temperatures, the energy obtained from quantum simulations for the different carbon isotopes converges to that of classical simulations, but at $T = 800$ K we still observe an appreciable difference between quantum and classical energy values. This is not strange, since the Debye temperature of graphene turns out to be $\Theta_D^{\text{out}} \gtrsim 1000$ K for out-of-plane modes [34, 35] and $\Theta_D^{\text{in}} \gtrsim 2000$ K for in-plane modes [34, 36], as indicated in the Introduction.

To make contact of our simulation results with a microscopic view based on the atomic vibrations, we consider a harmonic approximation (HA) for the vibrational modes of graphene. For a pure HA, the vibrational energy per atom of graphene is given by

$$E_{\text{int}}^{\text{HA}} = \frac{1}{N} \sum_{r,\mathbf{k}} \frac{1}{2} \hbar \omega_r(\mathbf{k}) \coth \left[\frac{1}{2} \beta \hbar \omega_r(\mathbf{k}) \right], \quad (9)$$

where the index r ($= 1, \dots, 6$) refers to the phonon bands: two branches with atomic displacements along the z direction (ZA and ZO), and four bands with in-plane displacements (LA, TA, LO, and TO) [68]. Here $\mathbf{k} = (k_x, k_y)$ are wavevectors in the 2D hexagonal Brillouin zone of the reciprocal lattice associated to the simulation cell with size N [30, 68–70]. The frequencies $\omega_r(\mathbf{k})$ correspond to the minimum-energy configuration of graphene (energy E_0), as derived from a diagonalization of the dynamical matrix for the LCBOPII potential. Note that for a HA of the vibrational modes, one has $E_{\text{kin}} = E_{\text{pot}}$ (virial theorem [49, 71]) for all temperatures in both classical and quantum approaches.

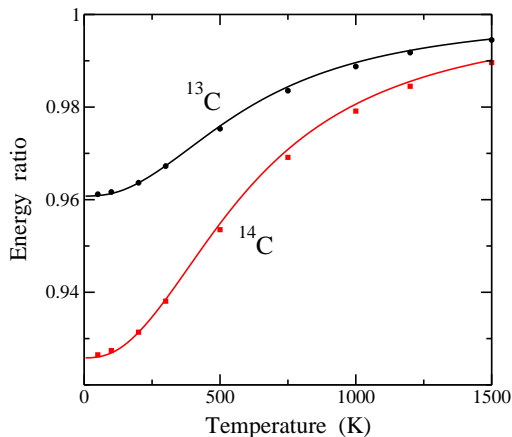


FIG. 2: Ratio between the internal energy of graphene for different carbon isotopes: $E_{\text{int}}^{13}/E_{\text{int}}^{12}$ (circles) and $E_{\text{int}}^{14}/E_{\text{int}}^{12}$ (squares). Error bars are less than the symbol size. Solid lines represent energy ratios corresponding to the harmonic approximation described in text (see Eq. (9)).

In the limit $T \rightarrow 0$, one has the zero-point energy:

$$E_{\text{int}}^0 = \frac{1}{N} \sum_{r,\mathbf{k}} \frac{1}{2} \hbar \omega_r(\mathbf{k}). \quad (10)$$

Taking into account that the frequencies $\omega_r(\mathbf{k})$ scale with isotopic mass as $M^{-1/2}$, at low T the ratio between internal energies for masses M_1 and M_2 converges to $(M_2/M_1)^{1/2}$ in the HA. On the other side, in the high-temperature limit, i.e., $\hbar \omega_r(\mathbf{k})/k_B T \ll 1$ for all $\omega_r(\mathbf{k})$, we have $E_{\text{int}} \rightarrow 3k_B T$ and the internal energy converges to the classical value, which is independent of the isotopic mass.

The behavior predicted by the HA for the energy ratio between different isotopes is basically what we find from PIMD simulations of graphene. In Fig. 2 we present the ratio between the internal energy of graphene for the carbon isotopes, as derived from PIMD simulations: $E_{\text{int}}^{13}/E_{\text{int}}^{12}$ (circles) and $E_{\text{int}}^{14}/E_{\text{int}}^{12}$ (squares). For comparison, we also show as solid lines the energy ratios obtained by using the HA given by Eq. (9). At low temperature, the energy ratios derived from the simulations converge to values close to the harmonic expectancy. For increasing temperature, the results of the PIMD simulations lie below those of the HA, and both sets of results approach each other for ^{13}C and ^{14}C at high T , as they converge to the classical limit (energy ratio equal to unity, irrespective of the anharmonicity).

V. ATOMIC MEAN-SQUARE DISPLACEMENTS

In this section we present results for the mean-square displacements of C atoms in graphene, yielded by PIMD simulations. These MSDs depend on the isotopic mass,

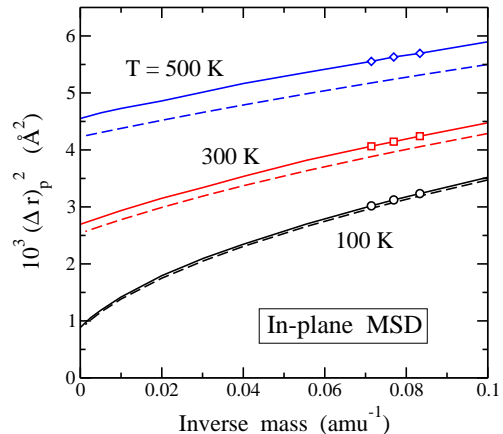


FIG. 3: In-plane MSD of carbon atoms vs inverse isotopic mass M^{-1} for $T = 100$ K (circles), 300 K (squares), and 500 K (diamonds). Solid lines were obtained from PIMD simulations of graphene with the LCBOP II potential for $N = 960$. Symbols correspond to actual carbon isotopes; from left to right: ^{14}C , ^{13}C , and ^{12}C . Dashed lines represent MSDs derived from the harmonic approximation described in the text. The classical limit corresponds to $M^{-1} \rightarrow 0$.

since the vibrational amplitudes are larger for smaller mass. In Fig. 3 we show the in-plane MSD of C atoms, $(\Delta r)_p^2$, as a function of the inverse isotopic mass $1/M$ for $T = 100$, 300 , and 500 K (solid lines). These data were obtained from PIMD simulations for different masses M . Symbols correspond to the actual carbon isotopes; from left to right: ^{14}C , ^{13}C , and ^{12}C . The limit $1/M \rightarrow 0$ (left part of the figure) corresponds to the classical limit.

For a given isotopic mass M , $(\Delta r)_p^2$ increases for rising temperature, as expected from the increase in vibrational amplitudes. Moreover, given a temperature T , the in-plane MSD rises from the classical limit as the atomic mass is lowered ($1/M$ rises). This increase is more important for lower temperature, as shown in Fig. 3 for $T = 100$ K, due to the larger importance of quantum effects at lower T .

The in-plane MSD at temperature T can be written in a HA as

$$(\Delta r)_p^2 \approx \frac{1}{N} \sum_{r,\mathbf{k}} \frac{\hbar}{2M\omega_r(\mathbf{k})} \coth\left(\frac{\hbar\omega_r(\mathbf{k})}{2k_B T}\right). \quad (11)$$

Here the index r ($= 1, \dots, 4$) runs over the phonon bands with in-plane atomic displacements (LA, TA, LO, and TO) [68]. Results of the HA are displayed in Fig. 3 as dashed lines. At $T = 100$ K these data follow closely those derived from PIMD simulations, and both sets of results depart one from the other at higher temperatures. This indicates an increase in the effect of anharmonicity on the in-plane MSD. The results of the simulations become larger than the prediction of the pure HA, but this approximation yields reasonable results at temperatures in the order of 100 K. The classical limit for the MSD is

given in a HA by:

$$C_p^2 \approx \frac{1}{N} \sum_{r,\mathbf{k}} \frac{k_B T}{M \omega_r(\mathbf{k})^2}, \quad (12)$$

and corresponds to the limit of $(\Delta r)_p^2$ on the left part of Fig. 3. In this classical approximation, C_p^2 is proportional to the temperature T .

For the out-of-plane displacements (z direction), it has been shown earlier that the character of the motion is predominantly classical above a crossover temperature T_c , which depends on the system size and decreases as N is raised [42]. This occurs because Q_z^2 decreases for rising temperature, while C_z^2 increases almost linearly with T , and the slope of $C_z^2(T)$ grows with system size N [42]. Increasing N gives rise to the onset of vibrational modes with longer wavelength λ . In fact, one can define an effective cut-off $\lambda_{max} \approx L$, with $L = (N A_p)^{1/2}$ (A_p : in-plane area per atom, see below). Calling $k = |\mathbf{k}|$, this translates into $k_{min} = 2\pi/\lambda_{max}$, i.e., $k_{min} \sim N^{-1/2}$.

For $N = 960$, the crossover for the out-of-plane motion occurs at $T_c \approx 10$ K [42], so for the temperatures considered here the atomic MSD in the z direction is basically controlled by the classical contribution C_z^2 , i.e., we have $C_z^2 \gg Q_z^2$. This is mainly due to low-frequency out-of-plane modes (*flexural* ZA band), which cause large vibrational amplitudes, and behave classically at the temperatures considered here. Thus, at a given temperature, changes in $(\Delta z)^2$ for the different carbon isotopes are expected to be negligible, since classical-like motion yields MSDs independent of the mass. We have checked this from the results of our PIMD simulations, and found that differences in the out-of-plane MSDs for different carbon isotopes are less than the statistical error bars. This means that, at least for the temperatures considered here ($T \geq 50$ K), the isotopic effects in the interatomic distances and in-plane area presented below are basically controlled by the atomic in-plane motion.

VI. INTERATOMIC DISTANCES

In this section we study changes of interatomic distances in graphene with temperature and isotopic mass. The temperature dependence of the equilibrium C–C distance, d_{C-C} , derived from PIMD simulations is shown in Fig. 4 for the different carbon isotopes: ^{12}C (circles), ^{13}C (squares), and ^{14}C (diamonds). For ^{12}C we find in the low-temperature limit an interatomic distance of 1.4287 Å, which grows as temperature is raised, as expected for the thermal expansion of the graphene sheet. The interatomic distance corresponding to the minimum-energy configuration (flat graphene sheet with energy E_0) amounts to 1.4199 Å, which means that the zero-point expansion of the C–C bond for ^{12}C is $(\Delta d)_0 = 8.8 \times 10^{-3}$ Å, i.e., a 0.6% of the classical result. This value is larger than the whole vertical axis presented in Fig. 4.

The dashed line in Fig. 4 corresponds to the results of classical simulations, which display a dependence nearly

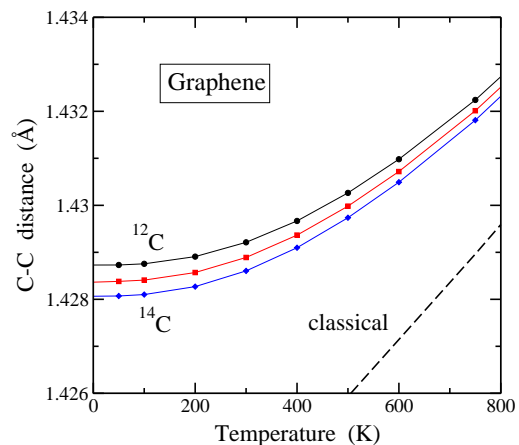


FIG. 4: Temperature dependence of the interatomic C–C distance in graphene for ^{12}C (circles), ^{13}C (squares), and ^{14}C (diamonds). Solid lines are guides to the eye. The dashed line represents results for d_{C-C} derived from classical MD simulations.

linear with temperature. A comparison between results derived from classical MD and PIMD simulations of graphene was presented in Ref. [42]. The bond expansion due to quantum zero-point motion was found to be in the order of the thermal expansion predicted by the classical model from $T = 0$ to 800 K. In the PIMD results, the rise in interatomic distance from $T = 0$ to 300 K is small, amounting to 5×10^{-4} Å, about 15 times smaller than the zero-point expansion $(\Delta d)_0$. The size effect of the finite simulation cell is negligible for our purposes [42]. For some selected temperatures, we have checked that results for d_{C-C} obtained for $N = 1560$ coincide within error bars with those presented here for $N = 960$.

The results for interatomic distances derived from classical and quantum simulations for a single layer of graphene are qualitatively similar to those found earlier for other carbon-based materials. For example, the zero-point expansion of the C–C bond for diamond was found to be $(\Delta d)_0 = 7.4 \times 10^{-3}$ Å, i.e., a 0.5% of the classical prediction [72].

For graphene, the C–C distance derived from PIMD simulations is found to decrease for increasing isotopic mass (see Fig. 4). At $T = 50$ K it is reduced by 3.5 and 6.6×10^{-4} Å for ^{13}C and ^{14}C , respectively, with respect to the C–C distance in ^{12}C . These differences are reduced for rising temperature, as nuclear quantum effects become less relevant. In Fig. 5 we display the temperature dependence of the ratio $\chi_M = (d_M - d_{12})/d_{12}$, where d_M is the interatomic distance corresponding to isotopic mass M . For ^{13}C and ^{14}C , this ratio converges for $T \rightarrow 0$ to -2.5×10^{-4} and -4.6×10^{-4} , respectively.

For diamond, it was found at low T a ratio $\chi_{13} = -1.8 \times 10^{-4}$ for ^{13}C , somewhat smaller than our result for graphene. This is most probably due to the different anharmonicity associated to the hybridization of carbon atoms in both materials: sp^3 in diamond vs sp^2 in

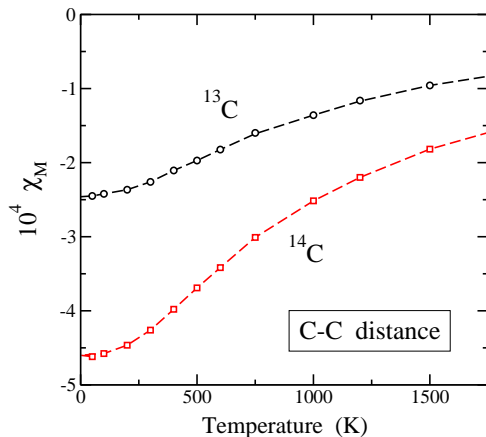


FIG. 5: Temperature dependence of $\chi_M = (d_M - d_{12})/d_{12}$ for ^{13}C (circles) and ^{14}C (squares), as derived from PIMD simulations of graphene. Dashed lines are guides to the eye. Error bars are in the order of the symbol size.

graphene. In fact, the thermal expansion of the interatomic distance (or lattice parameter) for diamond from $T = 0$ to 1000 K amounts to a 0.2%, vs a 0.4% for the expansion of $d_{\text{C-C}}$ in graphene [72].

The isotopic effect in the C–C distance studied here is clearly larger than the present sensitivity of diffraction techniques. Thus, for example, isotopic effects in lattice parameters and interatomic distances of crystalline materials can be measured with high precision using x-ray standing waves [73].

The zero-point dilation $(\Delta d)_0$ and the thermal bond expansion at $T > 0$ presented here are a consequence of anharmonicity in the interatomic potential, similar to 3D crystalline solids, e.g., diamond (see above). For graphene, this is mainly caused by anharmonicity in the stretching vibrations of the sp^2 C–C bond. A more complex anharmonic effect is the thermal variation of the graphene in-plane area, for the coupling between in-plane and out-of-plane vibrational modes, as discussed in Sec. VII.

In this section, we have analyzed the interatomic distances in isotopically pure graphene. As mentioned in Sec. III.A, one expects that structural variables for mixtures of carbon isotopes can be obtained from linear interpolation between those corresponding to isotopically pure samples. To check this point we have carried out some PIMD simulations for carbon mean mass of 12.25, 12.5, and 12.75 amu, and found that the results for the C–C distance coincide within error bars with those given from interpolation between the data obtained for $M = 12$ and 13 amu. Something similar happens for the in-plane area A_p discussed in the following section. In connection with this, we note that to calculate several properties of 3D crystals with isotopically mixed composition, it has been usually assumed that each atomic nucleus in the material has a mass equal to the average mass. This was called *virtual-crystal approximation* [13, 40, 46, 74], and

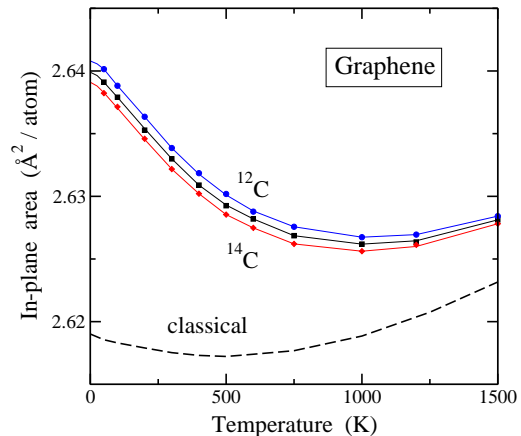


FIG. 6: In-plane area as a function of temperature for graphene made of different carbon isotopes: ^{12}C (circles), ^{13}C (squares), and ^{14}C (diamonds). These results were obtained from PIMD simulations for $N = 960$. The dashed line indicates the result for A_p obtained in classical MD simulations.

it has been found to give results that coincide with those yielded by simulations in which real isotopic mixtures are considered [13].

VII. LAYER AREA

The simulations presented here have been performed in the isothermal-isobaric ensemble, as indicated in Sec. III.A. Thus, for a given isotopic mass M , in a simulation run we fix the number of carbon atoms N , the temperature T , and the applied stress in the (x, y) plane (here $P = 0$), allowing for variations in the area of the simulation cell. In the following we will call A_p the in-plane area per C atom.

In the simulations, carbon atoms are allowed to freely move in the z coordinate (out-of-plane direction), so that the *real* surface of a graphene layer is not strictly planar, and has an area (in 3D space) larger than the in-plane area [42, 75]. The difference between the *real* area A and the *in-plane* area A_p (called *excess* [76–78] or *hidden* area [79]) has been discussed earlier for biological membranes [80–82], and more recently for crystalline membranes such as graphene [78, 83]. The *real* area A can be calculated from PIMD simulations of graphene by a triangulation based on the atomic positions [83, 84]. This area A is larger than A_p , and the difference between both increases with temperature, since the actual surface becomes increasingly bent as temperature is raised and out-of-plane atomic displacements around the reference plane are larger. Here we will concentrate on the in-plane area A_p , as it is the variable conjugate to the external pressure P .

In Fig. 6 we show the temperature dependence of A_p , as derived from PIMD simulations for three carbon iso-

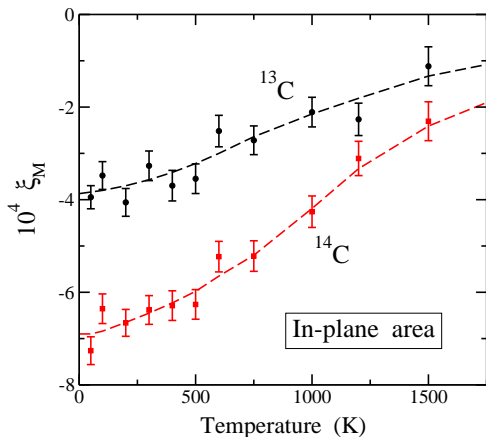


FIG. 7: Temperature dependence of $\xi_M = (A_p^M - A_p^{12})/A_p^{12}$ for ^{13}C (circles) and ^{14}C (squares), as derived from PIMD simulations of graphene. Dashed lines are guides to the eye.

topes: ^{12}C (circles), ^{13}C (squares), and ^{14}C (diamonds). In the three cases, A_p decreases for rising T , reaches a minimum at a temperature $T_m \sim 1000$ K, and increases at higher temperature. This behavior was found and discussed earlier for ^{12}C [42]. For comparison with the results of PIMD simulations, we also show in Fig. 6 the temperature dependence of A_p derived from classical MD simulations (dashed line). In the limit $T \rightarrow 0$, the difference between classical and quantum data for ^{12}C converges to $0.022 \text{ \AA}^2/\text{atom}$. This difference decreases for rising temperature, as nuclear quantum effects become less important. In particular, it is relevant that the decrease in A_p obtained from PIMD simulations from $T = 0$ to 1000 K is much larger than that found from classical molecular dynamics and Monte Carlo simulations [32, 42, 57, 85].

Given a temperature, the in-plane area A_p decreases for rising isotopic mass M , and eventually reaches the classical limit for large M . For $T = 50$ K, the decrease in A_p with respect to ^{12}C graphene amounts to $\Delta A_p = -1.0$ and $-1.9 \times 10^{-3} \text{ \AA}^2/\text{atom}$, for ^{13}C and ^{14}C , respectively. For the classical limit ($M \rightarrow \infty$), the shift is $-2.1 \times 10^{-2} \text{ \AA}^2/\text{atom}$.

The behavior of A_p as a function of temperature may be explained as a result of two competing factors. First, the real area A increases as temperature is raised, as happens for the interatomic distance $d_{\text{C-C}}$ shown in Fig. 4. Second, bending (rippling) of the graphene surface gives rise to a reduction of its 2D projection, i.e., A_p . At low temperature, this decrease due to out-of-plane motion dominates over the thermal expansion of the actual surface (which is small at low T), and then one has $dA_p/dT < 0$. At high temperature, the rise of the real area A dominates over the decrease in the projected area due to bending, and therefore $dA_p/dT > 0$. These arguments are similar to those given earlier to explain the results of classical simulations of graphene [85, 86].

Changes in interatomic distances and in the graphene area (both A and A_p) are important anharmonic effects. On one side, changes in the distance $d_{\text{C-C}}$ and in the real area A are mainly due to anharmonicity of the C-C stretching vibration. Moreover, out-of-plane vibrations cause fluctuations of the in-plane area and a decrease in its mean value.

In Fig. 7 we present the temperature dependence of the ratio $\xi_M = (A_p^M - A_p^{12})/A_p^{12}$, where A_p^M is the in-plane area for isotopic mass M . For ^{13}C and ^{14}C , this ratio converges at low T to $3.9(2) \times 10^{-4}$ and $6.9(2) \times 10^{-4}$, respectively. We note that the error bars in this case are clearly larger than for the ratio χ_M shown in Fig. 5 (not displayed for χ_M , as they are in the order of the symbol size). This is due to the larger statistical noise in A_p than in $d_{\text{C-C}}$ (or in the real area A), because of the larger fluctuations of the former at a given temperature. These fluctuations of A_p are due to the sluggish out-of-plane bending modes with the largest wavelengths (smallest k) and lowest vibrational frequencies corresponding to the considered simulation cell.

It is interesting to analyze the dependence of A_p on isotopic mass, from the actual carbon isotopes to the classical limit ($M \rightarrow \infty$), which is in fact obtained by carrying out classical MD simulations. This crossover can be actually visualized by plotting the in-plane area vs the inverse isotopic mass, $1/M$, at different temperatures, as displayed in Fig. 8. From top to bottom, lines represent A_p at several temperatures: 100, 300, 500, and 1000 K. In this plot, the left side $1/M \rightarrow 0$ corresponds to the classical limit, and symbols indicate the actual carbon isotopes: from left to right, ^{14}C , ^{13}C , and ^{12}C . Note that the line corresponding to $T = 1000$ K crosses the other lines for large M , since in the classical limit the minimum of A_p vs T appears at about 500 K [42]. Note that the difference in A_p between ^{12}C graphene and the classical limit changes from $2.1 \times 10^{-2} \text{ \AA}^2$ at 100 K to $7.8 \times 10^{-3} \text{ \AA}^2$ at 1000 K, in agreement with the results shown in Fig. 6.

The results of our PIMD simulations can be rationalized by analyzing the trends expected from a QHA for the vibrational modes in graphene. This method has been used earlier to study isotopic effects in structural properties of 3D solids [46, 47], and more recently in graphene [69]. In this approach, the frequencies $\omega_r(\mathbf{k})$ are assumed to change with the in-plane area, and for a given A_p the modes are treated as harmonic vibrations. Following these assumptions, and considering a reference mass M_{ref} (which is taken here as $M_{\text{ref}} = 12$ amu), the difference between in-plane areas for isotopic masses M and M_{ref} at $T = 0$, $\Delta A_p(0) = A_p^M(0) - A_p^{\text{ref}}(0)$, is given by the expression (see the Appendix):

$$\Delta A_p(0) = -\frac{1}{2} [A_p^{\text{ref}}(0) - A_0] \frac{\Delta M}{M_{\text{ref}}}, \quad (13)$$

with $\Delta M = M - M_{\text{ref}}$. This means that the low-temperature changes of A_p due to isotopic mass may be quantitatively explained from the change in A_p caused

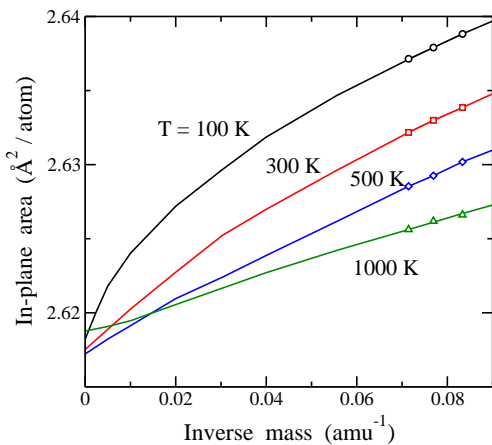


FIG. 8: In-plane area of graphene vs the inverse atomic mass M^{-1} for different temperatures: 100 K (circles), 300 K (squares), 500 K (diamonds), and 1000 K (triangles). The classical limit corresponds to $M^{-1} \rightarrow 0$.

by zero-point motion for the reference mass, i.e., from the difference $A_p^{\text{ref}}(0) - A_0$. Taking for this difference the value 0.022 \AA^2 (see above), Eq. (13) yields $\Delta A_p = -9.2 \times 10^{-4} \text{ \AA}^2$ and $-1.8 \times 10^{-3} \text{ \AA}^2$ for ^{13}C and ^{14}C , respectively. These values are very close to the low-temperature results found from direct calculation of the in-plane area corresponding to different atomic masses: -1.0 and $-1.8 \times 10^{-3} \text{ \AA}^2$, respectively.

One can also find an expression for the isotopic effect on A_p at high temperature ($T \gtrsim \Theta_D$, see the Appendix):

$$\Delta A_p(T) = - [A_p^{\text{ref}}(T) - A_p^{\text{cl}}(T)] \frac{\Delta M}{M_{\text{ref}}}. \quad (14)$$

This formula corresponding to high temperature is analogous to that given above for $T = 0$ [see Eq. (13)], the only difference between them being a factor 2 which appears in the denominator of the low-temperature formula. Expressions similar to Eq. (14) have been used to analyze the isotopic effect in the volume and interatomic distances in 3D solids such as silicon [48], at temperatures higher than the Debye temperature of the material. For graphene, we have for in-plane vibrational modes $\Theta_D^{\text{in}} \gtrsim 2000 \text{ K}$, a temperature higher than those studied here. In any case, at $T = 1500 \text{ K}$, Eq. (14) gives $\Delta A_p = -4.4$ and $-8.8 \times 10^{-3} \text{ \AA}^2$ for ^{13}C and ^{14}C , respectively, which turn out to be larger than those found directly from the PIMD simulations, i.e., -3.0 and $-6.1 \times 10^{-3} \text{ \AA}^2$, which confirms that the high- T approximation Eq. (14) overestimates the isotopic effect at $T = 1500 \text{ K} < \Theta_D^{\text{in}}$.

We finally note that the QHA yields reasonable predictions for the isotopic effect on the in-plane area, specially at low temperatures. Nevertheless, anharmonic force constants not included in this approximation can give rise to some anomalies in its predictions [69, 86].

VIII. SUMMARY

PIMD simulations are a powerful tool to study isotopic effects in condensed matter. This method allows one to study phonon-related properties, further than harmonic approximations for the vibrational modes, and explore their dependence on the mass of the constituent atoms, which appears as an input parameter in the calculations.

Here we have demonstrated the applicability of the PIMD method to analyze the dependence of structural properties of 2D materials on the atomic mass. In particular, we have studied the change of interatomic distances and in-plane area for different carbon isotopes in a wide range of temperatures, from $T = 50$ to 1500 K .

At low temperature, we find a relative change of the C–C distance in ^{13}C and ^{14}C graphene of -2.5 and -4.6×10^{-4} with respect to ^{12}C , respectively. For the in-plane area A_p , the corresponding relative changes amount to -3.9 and -6.9×10^{-4} . The magnitude of these isotopic effects decreases as temperature rises. Thus, for A_p in ^{13}C graphene we find a relative variation of -3.4 and -2.1×10^{-4} at 300 and 1000 K, respectively,

An interesting application of path-integral simulations is to study the evolution of structural properties of 2D materials by changing the atomic mass from the actual isotopic masses to the classical limit ($M \rightarrow \infty$), which is usually considered in atomistic simulations of this type of materials. This has been presented here for the in-plane MSD and in-plane area A_p of graphene at several temperatures in Figs. 3 and 8. A similar mass dependence is obtained for the interatomic C–C distance.

The classical limit is indeed useful to study mechanical and vibrational properties of graphene, but nuclear quantum effects have to be taken into account for a proper quantification of structural and thermodynamic variables. Classical simulations are, in fact, insensitive to the atomic mass and thereby to the isotopic effects discussed here.

Apart from isotopic effects in structural properties, the extent of anharmonicity has been quantified by comparing the internal energy and in-plane vibrational amplitudes with those obtained from a harmonic approximation. This is particularly observable in the in-plane MSD, $(\Delta r)_p^2$, shown in Fig. 3 with an increasing departure from the harmonic calculation for rising temperature. For ^{12}C , the difference between PIMD and HA results is about 1% at $T = 100 \text{ K}$ and amounts to a 7% at 500 K.

Path-integral simulations similar to those presented here can be useful to analyze isotopic effects in structural and vibrational properties of graphene (i.e., hydrogenated graphene), where the light mass of hydrogen can cause a larger departure of harmonicity than that found here for graphene. Another interesting topic may be the dependence of the isotopic effects discussed here on tensile external stress, which could be also studied in the isothermal-isobaric ensemble.

Acknowledgments

This work was supported by Ministerio de Ciencia e Innovación (Spain) through Grants FIS2015-64222-C2 and PGC2018-096955-B-C44.

Author contribution statement

All authors contributed equally to the paper

Appendix A: Quasiharmonic approximation

In a QHA for 3D solids, the vibrational modes are described by harmonic oscillators of frequencies $\omega_r(\mathbf{k})$, which depend on the volume of the crystal [46–48, 69]. For graphene, the in-plane area A_p plays the role of the volume in 3D crystals. Then, the equilibrium A_p for isotopic mass M at temperature T and zero external stress can be derived by a minimization of the Helmholtz free energy [69]. One finds

$$A_p^M(T) = A_0 + \frac{1}{NB_0} \sum_{r,\mathbf{k}} \gamma_r(\mathbf{k}) E_r(\mathbf{k}, T) , \quad (\text{A1})$$

where

$$E_r(\mathbf{k}, T) = \frac{1}{2} \hbar \omega_r(\mathbf{k}) \coth \left(\frac{\hbar \omega_r(\mathbf{k})}{2k_B T} \right) . \quad (\text{A2})$$

Here, $\omega_r(\mathbf{k})$ are the frequencies of the phonon band r , B_0 is the 2D modulus of hydrostatic compression [87], A_0 is the zero-temperature in-plane area in the limit of infinite isotopic mass (classical limit, $A_0 = A_p^{\text{cl}}(0)$), and

$$\gamma_r(\mathbf{k}) = - \left. \frac{\partial \ln \omega_r(\mathbf{k})}{\partial \ln A_p} \right|_0 \quad (\text{A3})$$

is the Grüneisen parameter of mode r, \mathbf{k} [8].

At $T = 0$ the difference $A_p^M(0) - A_0$ is given by

$$A_p^M(0) - A_0 = \frac{1}{2NB_0} \sum_{r,\mathbf{k}} \hbar \omega_r(\mathbf{k}) \gamma_r(\mathbf{k}) . \quad (\text{A4})$$

A first-order expansion for the in-plane area as a function of isotopic mass yields:

$$A_p^M(0) = A_p^{\text{ref}}(0) + \left. \frac{\partial A_p^M(0)}{\partial M} \right|_{M_{\text{ref}}} \Delta M , \quad (\text{A5})$$

with $\Delta M = M - M_{\text{ref}}$ the mass increment with respect to a reference mass, which is taken here as $M_{\text{ref}} = 12$ amu. Taking into account that the frequencies $\omega_r(\mathbf{k})$ scale with isotopic mass as $M^{-1/2}$, we have

$$\frac{\partial \omega_r(\mathbf{k})}{\partial M} = - \frac{\omega_r(\mathbf{k})}{2M} , \quad (\text{A6})$$

and

$$\frac{\partial A_p^M(0)}{\partial M} = - \frac{1}{2M} [A_p^M(0) - A_0] . \quad (\text{A7})$$

Thus, at $T = 0$ one has for the change of in-plane area due to isotopic mass:

$$\Delta A_p(0) = - \frac{1}{2} [A_p^{\text{ref}}(0) - A_0] \frac{\Delta M}{M_{\text{ref}}} . \quad (\text{A8})$$

At high temperatures, the difference $A_p^M(T) - A_p^{\text{ref}}(T)$ can be also expressed as a function of the difference $A_p^{\text{ref}}(T) - A_p^{\text{cl}}(T)$ between the in-plane area for the reference mass M_{ref} and that corresponding to the classical limit ($M \rightarrow \infty$) at temperature T . In a QHA, we have:

$$A_p^M(T) - A_p^{\text{cl}}(T) = \frac{1}{NB_0} \sum_{r,\mathbf{k}} \gamma_r(\mathbf{k}) [E_r(\mathbf{k}, T) - k_B T] . \quad (\text{A9})$$

Using a high-temperature expansion for the energy $E_r(\mathbf{k}, T)$ given in Eq. (A2), one finds for $T \gtrsim \Theta_D$:

$$A_p^M(T) - A_p^{\text{cl}}(T) = \frac{1}{12NB_0 k_B T} \sum_{r,\mathbf{k}} \gamma_r(\mathbf{k}) [\hbar \omega_r(\mathbf{k})]^2 , \quad (\text{A10})$$

which indicates that the isotopic effect on the in-plane area decreases for rising temperature as $1/T$.

From Eq. (A10), and using a first-order expansion for $\Delta A_p(T)$ as a function of ΔM , analogous to that given above for $T = 0$ in Eq. (A5), one finds

$$\Delta A_p(T) = - [A_p^{\text{ref}}(T) - A_p^{\text{cl}}(T)] \frac{\Delta M}{M_{\text{ref}}} . \quad (\text{A11})$$

This expression corresponding to high temperature is similar to that found for $T = 0$ [see Eq. (A8)]. The difference between them is a factor 2 appearing in the denominator of the low-temperature expression.

-
- [1] A. K. Geim and K. S. Novoselov, *Nature Mater.* **6**, 183 (2007).
 [2] G. W. Flynn, *J. Chem. Phys.* **135**, 050901 (2011).
 [3] C. Lee, X. Wei, J. W. Kysar, and J. Hone, *Science* **321**, 385 (2008).

- [4] S. Ghosh, I. Calizo, D. Teweldebrhan, E. P. Pokatilov, D. L. Nika, A. A. Balandin, W. Bao, F. Miao, and C. N. Lau, *Appl. Phys. Lett.* **92**, 151911 (2008).
 [5] D. L. Nika, E. P. Pokatilov, A. S. Askerov, and A. A. Balandin, *Phys. Rev. B* **79**, 155413 (2009).

- [6] A. A. Balandin, *Nature Mater.* **10**, 569 (2011).
- [7] J. C. Meyer, A. K. Geim, M. I. Katsnelson, K. S. Novoselov, T. J. Booth, and S. Roth, *Nature* **446**, 60 (2007).
- [8] N. W. Ashcroft and N. D. Mermin, *Solid State Physics* (Saunders College, Philadelphia, 1976).
- [9] C. Kittel, *Introduction to Solid State Physics* (Wiley, New York, 1996), 7th ed.
- [10] R. Ramírez and C. P. Herrero, *J. Chem. Phys.* **133**, 144511 (2010).
- [11] M. Cardona, P. Etchegoin, H. Fuchs, and P. Molinas-Mata, *J. Phys.: Condens. Matter* **5**, A61 (1993).
- [12] M. Cardona, *Phys. Status Solidi B* **220**, 5 (2000).
- [13] C. P. Herrero, R. Ramírez, and M. Cardona, *Phys. Rev. B* **79**, 012301 (2009).
- [14] C. P. Herrero and R. Ramírez, *J. Chem. Phys.* **134**, 094510 (2011).
- [15] S. Bernard, E. Whiteway, V. Yu, D. G. Austing, and M. Hilke, *Phys. Rev. B* **86**, 085409 (2012).
- [16] S. Broderick, U. Ray, S. Srinivasan, K. Rajan, and G. Balasubramanian, *Appl. Phys. Lett* **104**, 243110 (2014).
- [17] J. F. Rodríguez-Nieva, R. Saito, S. D. Costa, and M. S. Dresselhaus, *Phys. Rev. B* **85**, 245406 (2012).
- [18] E. del Corro, M. Kalbac, C. Fantini, O. Frank, and M. A. Pimenta, *Phys. Rev. B* **88**, 155436 (2013).
- [19] B. R. Carvalho, Y. Hao, A. Righi, J. F. Rodríguez-Nieva, L. Colombo, R. S. Ruoff, M. A. Pimenta, and C. Fantini, *Phys. Rev. B* **92**, 125406 (2015).
- [20] J. Hu, S. Schiffl, A. Vallabhaneni, X. Ruan, and Y. P. Chen, *Appl. Phys. Lett* **97**, 133107 (2010).
- [21] J.-W. Jiang, J. Lan, J.-S. Wang, and B. Li, *J. Appl. Phys.* **107**, 054314 (2010).
- [22] V. Adamyan and V. Zavalniuk, *J. Phys.: Condens. Matter* **24**, 415401 (2012).
- [23] M. Davies, B. Ganapathysubramanian, and G. Balasubramanian, *Appl. Phys. Lett* **110**, 133107 (2017).
- [24] P. L. de Andres, F. Guinea, and M. I. Katsnelson, *Phys. Rev. B* **86**, 245409 (2012).
- [25] G. M. Chechin, S. V. Dmitriev, I. P. Lobzenko, and D. S. Ryabov, *Phys. Rev. B* **90**, 045432 (2014).
- [26] E. Cadelano, P. L. Palla, S. Giordano, and L. Colombo, *Phys. Rev. Lett.* **102**, 235502 (2009).
- [27] G.-D. Lee, E. Yoon, N.-M. Hwang, C.-Z. Wang, and K.-M. Ho, *Appl. Phys. Lett.* **102**, 021603 (2013).
- [28] C. P. Herrero and R. Ramírez, *Phys. Rev. B* **79**, 115429 (2009).
- [29] A. Fasolino, J. H. Los, and M. I. Katsnelson, *Nature Mater.* **6**, 858 (2007).
- [30] R. Ramírez, E. Chacón, and C. P. Herrero, *Phys. Rev. B* **93**, 235419 (2016).
- [31] Y. Magnin, G. D. Foerster, F. Rabilloud, F. Calvo, A. Zappelli, and C. Bichara, *J. Phys.: Condens. Matter* **26**, 185401 (2014).
- [32] B. G. A. Brito, L. Cândido, G.-Q. Hai, and F. M. Peeters, *Phys. Rev. B* **92**, 195416 (2015).
- [33] J. H. Los, A. Fasolino, and M. I. Katsnelson, *Phys. Rev. Lett.* **116**, 015901 (2016).
- [34] V. K. Tewary and B. Yang, *Phys. Rev. B* **79**, 125416 (2009).
- [35] A. Politano, B. Borca, M. Minniti, J. J. Hinarejos, A. L. Vazquez de Parga, D. Farias, and R. Miranda, *Phys. Rev. B* **84**, 035450 (2011).
- [36] E. Pop, V. Varshney, and A. K. Roy, *MRS Bull.* **37**, 1273 (2012).
- [37] C. P. Herrero, *Phys. Rev. B* **65**, 014112 (2002).
- [38] M. H. Müser, P. Nielaba, and K. Binder, *Phys. Rev. B* **51**, 2723 (1995).
- [39] J. C. Noya, C. P. Herrero, and R. Ramírez, *Phys. Rev. B* **56**, 237 (1997).
- [40] C. P. Herrero, *Solid State Commun.* **110**, 243 (1999).
- [41] J. H. Los, M. I. Katsnelson, O. V. Yazyev, K. V. Zakharchenko, and A. Fasolino, *Phys. Rev. B* **80**, 121405 (2009).
- [42] C. P. Herrero and R. Ramírez, *J. Chem. Phys.* **145**, 224701 (2016).
- [43] C. Cohen-Tannoudji, B. Liu, and F. Lalöe, *Quantum Mechanics*, vol. 1 (Wiley, New York, 1977).
- [44] F. Reif, *Fundamentals of statistical and thermal physics* (McGraw-Hill, New York, 1965).
- [45] W. Greiner, L. Neise, and H. Stöcker, *Thermodynamics and statistical mechanics* (Springer, New York, 1995).
- [46] A. Debernardi and M. Cardona, *Phys. Rev. B* **54**, 11305 (1996).
- [47] N. Garro, A. Cantarero, M. Cardona, A. Gobel, T. Ruf, and K. Eberl, *Phys. Rev. B* **54**, 4732 (1996).
- [48] C. P. Herrero, *Phys. Status Solidi B* **220**, 857 (2000).
- [49] R. P. Feynman, *Statistical Mechanics* (Addison-Wesley, New York, 1972).
- [50] M. J. Gillan, *Phil. Mag. A* **58**, 257 (1988).
- [51] D. M. Ceperley, *Rev. Mod. Phys.* **67**, 279 (1995).
- [52] C. P. Herrero and R. Ramírez, *J. Phys.: Condens. Matter* **26**, 233201 (2014).
- [53] J. H. Los and A. Fasolino, *Phys. Rev. B* **68**, 024107 (2003).
- [54] J. H. Los, L. M. Ghiringhelli, E. J. Meijer, and A. Fasolino, *Phys. Rev. B* **72**, 214102 (2005).
- [55] L. M. Ghiringhelli, C. Valeriani, J. H. Los, E. J. Meijer, A. Fasolino, and D. Frenkel, *Mol. Phys.* **106**, 2011 (2008).
- [56] L. M. Ghiringhelli, J. H. Los, A. Fasolino, and E. J. Meijer, *Phys. Rev. B* **72**, 214103 (2005).
- [57] K. V. Zakharchenko, M. I. Katsnelson, and A. Fasolino, *Phys. Rev. Lett.* **102**, 046808 (2009).
- [58] K. V. Zakharchenko, A. Fasolino, J. H. Los, and M. I. Katsnelson, *J. Phys.: Condens. Matter* **23**, 202202 (2011).
- [59] A. Politano, A. R. Marino, D. Campi, D. Fariás, R. Miranda, and G. Chiarello, *Carbon* **50**, 4903 (2012).
- [60] P. Lambin, *Appl. Sci.* **4**, 282 (2014).
- [61] M. E. Tuckerman, B. J. Berne, and G. J. Martyna, *J. Chem. Phys.* **97**, 1990 (1992).
- [62] M. E. Tuckerman, *Statistical Mechanics: Theory and Molecular Simulation* (Oxford University Press, Oxford, 2010).
- [63] G. J. Martyna, A. Hughes, and M. E. Tuckerman, *J. Chem. Phys.* **110**, 3275 (1999).
- [64] G. J. Martyna, M. E. Tuckerman, D. J. Tobias, and M. L. Klein, *Mol. Phys.* **87**, 1117 (1996).
- [65] C. P. Herrero, R. Ramírez, and E. R. Hernández, *Phys. Rev. B* **73**, 245211 (2006).
- [66] M. F. Herman, E. J. Bruskin, and B. J. Berne, *J. Chem. Phys.* **76**, 5150 (1982).
- [67] R. Ramírez, N. Neuerburg, M. V. Fernández-Serra, and C. P. Herrero, *J. Chem. Phys.* **137**, 044502 (2012).
- [68] R. Ramírez and C. P. Herrero, *J. Chem. Phys.* **151**, 224107 (2019).
- [69] N. Mounet and N. Marzari, *Phys. Rev. B* **71**, 205214 (2005).

- [70] L. J. Karssemeijer and A. Fasolino, *Surf. Sci.* **605**, 1611 (2011).
- [71] L. D. Landau and E. M. Lifshitz, *Statistical Physics* (Pergamon, Oxford, 1980), 3rd ed.
- [72] C. P. Herrero and R. Ramírez, *Phys. Rev. B* **63**, 024103 (2000).
- [73] A. Kazimorov, J. Zegenhagen, and M. Cardona, *Science* **282**, 930 (1998).
- [74] M. Cardona and M. L. W. Thewalt, *Rev. Mod. Phys.* **77**, 1173 (2005).
- [75] K. R. Hahn, C. Melis, and L. Colombo, *J. Phys. Chem. C* **120**, 3026 (2016).
- [76] W. Helfrich and R. M. Servuss, *Nuovo Cimento D* **3**, 137 (1984).
- [77] J.-B. Fournier and C. Barbetta, *Phys. Rev. Lett.* **100**, 078103 (2008).
- [78] C. P. Herrero and R. Ramírez, *Phys. Rev. B* **101**, 035405 (2020).
- [79] R. J. T. Nicholl, N. V. Lavrik, I. Vlassiuk, B. R. Srijanto, and K. I. Bolotin, *Phys. Rev. Lett.* **118**, 266101 (2017).
- [80] A. Imparato, *J. Chem. Phys.* **124**, 154714 (2006).
- [81] Q. Waheed and O. Edholm, *Biophys. J.* **97**, 2754 (2009).
- [82] E. Chacón, P. Tarazona, and F. Bresme, *J. Chem. Phys.* **143**, 034706 (2015).
- [83] R. Ramírez and C. P. Herrero, *Phys. Rev. B* **95**, 045423 (2017).
- [84] C. P. Herrero and R. Ramírez, *J. Chem. Phys.* **150**, 204707 (2019).
- [85] W. Gao and R. Huang, *J. Mech. Phys. Solids* **66**, 42 (2014).
- [86] K. H. Michel, S. Costamagna, and F. M. Peeters, *Phys. Status Solidi B* **252**, 2433 (2015).
- [87] F. Behroozi, *Langmuir* **12**, 2289 (1996).